analytical chemistry

Subscriber access provided by UNIV OF WESTERN ONTARIO

Article

Resolved Infrared Spectroscopy of Aqueous Molecules Employing Tunable Graphene Plasmons in Otto Prism

Jinpeng Nong, Wei Wei, Guilian Lan, Peng Luo, Caicheng Guo, Jue-Min Yi, and Linlong Tang

Anal. Chem., **Just Accepted Manuscript** • DOI: 10.1021/acs.analchem.0c02733 • Publication Date (Web): 22 Sep 2020

Downloaded from pubs.acs.org on October 12, 2020

Just Accepted

"Just Accepted" manuscripts have been peer-reviewed and accepted for publication. They are posted online prior to technical editing, formatting for publication and author proofing. The American Chemical Society provides "Just Accepted" as a service to the research community to expedite the dissemination of scientific material as soon as possible after acceptance. "Just Accepted" manuscripts appear in full in PDF format accompanied by an HTML abstract. "Just Accepted" manuscripts have been fully peer reviewed, but should not be considered the official version of record. They are citable by the Digital Object Identifier (DOI®). "Just Accepted" is an optional service offered to authors. Therefore, the "Just Accepted" Web site may not include all articles that will be published in the journal. After a manuscript is technically edited and formatted, it will be removed from the "Just Accepted" Web site and published as an ASAP article. Note that technical editing may introduce minor changes to the manuscript text and/or graphics which could affect content, and all legal disclaimers and ethical guidelines that apply to the journal pertain. ACS cannot be held responsible for errors or consequences arising from the use of information contained in these "Just Accepted" manuscripts.

is published by the American Chemical Society. 1155 Sixteenth Street N.W., Washington, DC 20036

Published by American Chemical Society. Copyright © American Chemical Society. However, no copyright claim is made to original U.S. Government works, or works produced by employees of any Commonwealth realm Crown government in the course of their duties.

Resolved Infrared Spectroscopy of Aqueous Molecules Employing Tunable Graphene Plasmons in Otto Prism

Jinpeng Nong [a,b], Wei Wei [a,b,*], Guilian Lan [a], Peng Luo [a], Caicheng Guo [a], Juemin Yi [c], and Linlong Tang [b,*]

[1] Key Laboratory of Optoelectronic Technology & Systems, Ministry of Education of China, College of Optoelectronic Engineering, Chongqing University, Chongqing, 400044, P.R. China

[2] Chongqing Key Laboratory of Multi-scale Manufacturing Technology, Chongqing Institute of Green and Intelligent Technology, Chinese Academy of Sciences, Chongqing 400714, P.R. China.

[3] Institut für Physik, Carl von Ossietzky Universität, D-26111 Oldenburg, Germany

* Corresponding authors, E-mail: tll@cigit.ac.cn, wwei@cqu.edu.cn

KEYWORDS: graphene, plasmons, surface enhanced infrared absorption spectroscopy, attenuated total reflection, aqueous molecules.

ABSTRACT: Real-time and *in situ* detection of aqueous solution is essential for bioanalysis and chemical reactions. However, it is extremely challenging for the infrared microscopic measurement due to the large background of water absorption. Here, we proposed a wideband tunable graphene plasmonic infrared biosensor to detect the biomolecules in aqueous environment, employing attenuated total reflection in an Otto prism configuration and tightly confined plasmons in graphene nanoribbons. Benefited from the graphene plasmonic electric field enhancement, such biosensor is able to identify the molecular chemical fingerprints without the interference of water absorption. As a proof of concept, the recombinant protein AG and goat anti-mouse immunoglobulin G (IgG) is used as the sensing analyte, of which the vibrational modes (1669 cm^{-1} and 1532 cm^{-1}) are very close to the OH-bending mode of water (1640 cm^{-1}). Simulation results show that the fingerprints of protein molecules in water environment can be selectively enhanced. Therefore, the water absorption is successfully suppressed so that two protein modes can be resolved by sweeping graphene Fermi energy in a wide waveband. By further optimizing the incident angle and graphene mobility to improve the mode energy of graphene plasmons, maximum enhancement factor of 112 and 130 can be achieved for Amide I and II bands. Our work provides an effective approach for the highly sensitive and selective *in situ* identification of aqueous-phase molecular fingerprints in fields of healthcare, food safety and biochemical sensing.

Infrared spectroscopy[1, 2]can quantitatively and qualitatively recognize the chemical groups inside molecules by detecting the structural vibrations from the infrared fingerprint spectrum. It possesses the advantages of real time, non-destructive and label-free, which has shown great potential in healthcare, food safety and biochemical sensing in the past few decades[3, 4]. Unfortunately, the sensitivity of traditional infrared spectroscopy is limited due to the small infrared absorption cross-sections of ultrathin films induced by the giant scale mismatch between microscale infrared light and nanoscale molecules, severely restricting its applications for the detection of trace level samples. To address this issue, surface-enhanced infrared absorption spectroscopy (SEIRAS) employing metallic plasmonic resonance with strong electromagnetic near-field confinement has been developed[2, 5]. The key point for this technology is to design an infrared resonant antenna with a specific plasmonic frequency. Benefited from the rapid development of micro-nano fabrication technology, various well-engineered metallic IR plasmonic microantennas have been designed for SEIRAS[2, 6, 7], such as coupled arrays of antennas[8, 9], fractal-shaped antennas[10] and perfect absorber structures[11, 12]. By tuning the frequencies of such plasmonic antennas into the fingerprint region and overlap with the infrared absorption frequencies of molecules, the vibrational signal of trace level samples can be significantly enlarged. Despite these progresses, noble metal plasmonic antennas still cannot fully satisfy the required enhancement to address the ongoing challenges and emerging applications hindered by the shortcomings of narrow spectral linewidth, weak near-field confinement, and limited tunable resonance.

Graphene[13, 14], a two-dimensional material consisted of carbon atoms arranged in a honeycomb pattern, has been proposed to be a promising alternative plasmonic material for SEIRAS owing to its remarkable optoelectronic properties[15]. Compared to the metallic microantennas, graphene nanoantennas can support tightly confined plasmon modes in infrared region with mode volumes several orders smaller than the excitation wavelength[16-20]. Particularly, such plasmonic responses can be dynamically tuned over the infrared region by external gate voltage[21-27],

which enables the selective enhancement of molecular infrared vibrational fingerprints. So far, graphene plasmons based SEIRAS have been successfully applied in various situations for the detection of vibrational modes with high sensitivity, significantly promoting the development of far-field infrared spectroscopies[1]. Yet, these reported graphene plasmon enhanced infrared sensors are mainly focused on solid (e.g., PMMA[28], PEO polymer[29, 30], silk[31], and protein film[32, 33]) and gas (e.g. SO_2, NO, NO_2)[34, 35] detections. For the molecules detection in aqueous solution, the infrared signal of the molecules could be overwhelmed by the large background absorption from water, which is difficult to avoid since the measurements of infrared spectra are usually performed under a transmission mode[36]. This significantly restricts the practical application of graphene plasmon enhanced infrared sensors for real-time and in situ detection of molecules in aqueous solution, which is of great importance for bioanalysis because the biomolecules are only active in aqueous solution and many life-sustaining biochemical reactions can only occur in aqueous environment.

In this paper, we theoretically proposed a wideband tunable graphene plasmon-enhanced infrared biosensor in combination of double layer graphene nanoribbon and an Otto prism configuration. In such configuration, the spacer can be served as the gating dielectric to tune the Fermi energy of graphene, while double layer graphene is used to achieve a higher Fermi energy and a larger tunable range. We show that graphene plasmons with strong near-field enhancement can effectively suppress the background water absorption under the attenuated total reflection (ATR) condition, which enables us to detect the target molecules in aqueous solution via ATR-SEIRAS. As an illustration for biosensing, the recombinant protein A/G and goat anti-mouse immunoglobulin G (IgG) are used as the sensing analyte in water environment to evaluate the performance of the sensing platform. By sweeping the graphene Fermi energy, the chemical fingerprints of the protein molecules can be recognized and resolved without the interference of water in a wideband.

METHOD SECTION

Design of the sensor. The schematic of the proposed wideband tunable graphene plasmon-enhanced ATR-SEIRAS based on Otto prism configuration is sketched in Figure 1(a). From top to bottom are double layer graphene nanoribbons with period of Λ and width of W, the dielectric spacer layer with thickness of t, and the prism. Here, an Otto configuration instead of a Kretschrnann configuration is used since the spacer can be served as the gating dielectric to tune the Fermi energy of graphene, which is unavailable in the Kretschrnann configuration. While double layer graphene is used to achieve a stronger plasmonic response since it can be regarded as monolayer graphene with an equivalent higher doping[37]. In practice, such configuration may be fabricated by the following steps. Firstly, the large-area monolayer graphene can be synthesized on cupper foil by a common-used Chemical Vapor Deposition method. Subsequently, two graphene layers are successively transferred from cupper foil onto an Otto prism configuration by a PMMA-assisted method. Finally, the

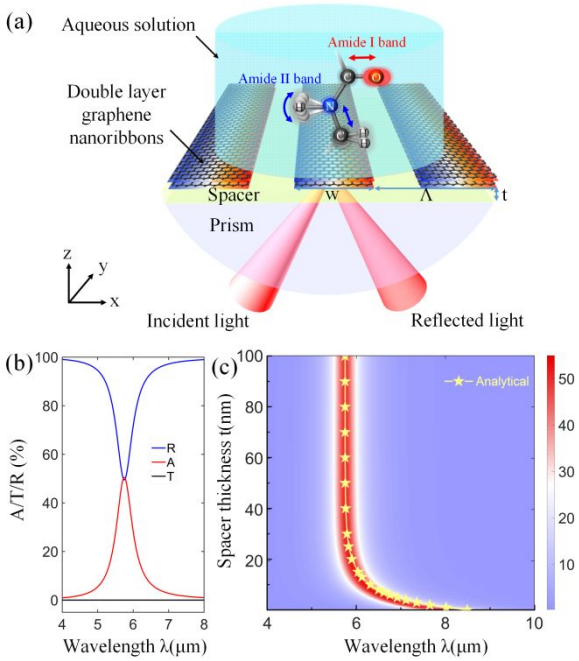

Figure 1 (a) Schematics of graphene plasmonic based ATR-SEIRAS configuration for aqueous molecules detection. (b) The absorption, transmission and reflection spectra when θ=40deg, Λ=100nm, W=50nm, t=50nm, E_f =0.4eV, N=2 and μ_c =1000 $cm^2V^{-1}s^{-1}$. (c) Absorption mapping as a function of the spacer thickness and incident wavelength. The star yellow line shown the analytical result.

graphene plasmonic nanostructure can be fabricated by Nano-printing technique. Compared with the SEIRAS measurement in traditional transmission configuration, such ATR configuration allows us to detect the target molecules dissolved even in strongly infrared absorbing media, such as water, since the shallow penetration depth (i.e., few micrometers) of infrared light into the surrounding media[38-41]. Especially, the near-field enhancement of graphene plasmons could further shrink the original evanescent wavelength, which minimizes the optical path to an extreme subwavelength level and significantly suppresses the signal from the bulk water molecules.

Modeling of the sensor. Simulations were performed using *Comsol Multiphysics*. Graphene is modelled as the surface current density boundary condition using the surface conductivity $\sigma(\omega)$ characterized by a Drude-like formula in the considered infrared region as[42-44]

$$\sigma(\omega) = N\frac{e^2 E_f}{\pi\hbar^2}\frac{i}{\omega + i\tau^{-1}} \quad (1)$$

where N is the number of graphene layers, e is the elementary charge, E_f is the Fermi energy, $\hbar$ is the reduced Planck constant, τ is the electron relaxation time defined as $\tau=\mu E_f/ev_f^2$, $v_f=c/300$ is the Fermi velocity, c is the speed of light in vacuum and μ is the carrier mobility of graphene. In the simulations, the Bloch periodic boundary condition is applied in the x-direction, while the perfectly matched-layer is imposed at two ends of computational space to achieve the absorbing boundary conditions in z-direction. A transverse magnetic polarized light with electric field intensity of 1V/m irradiates upon the structure with

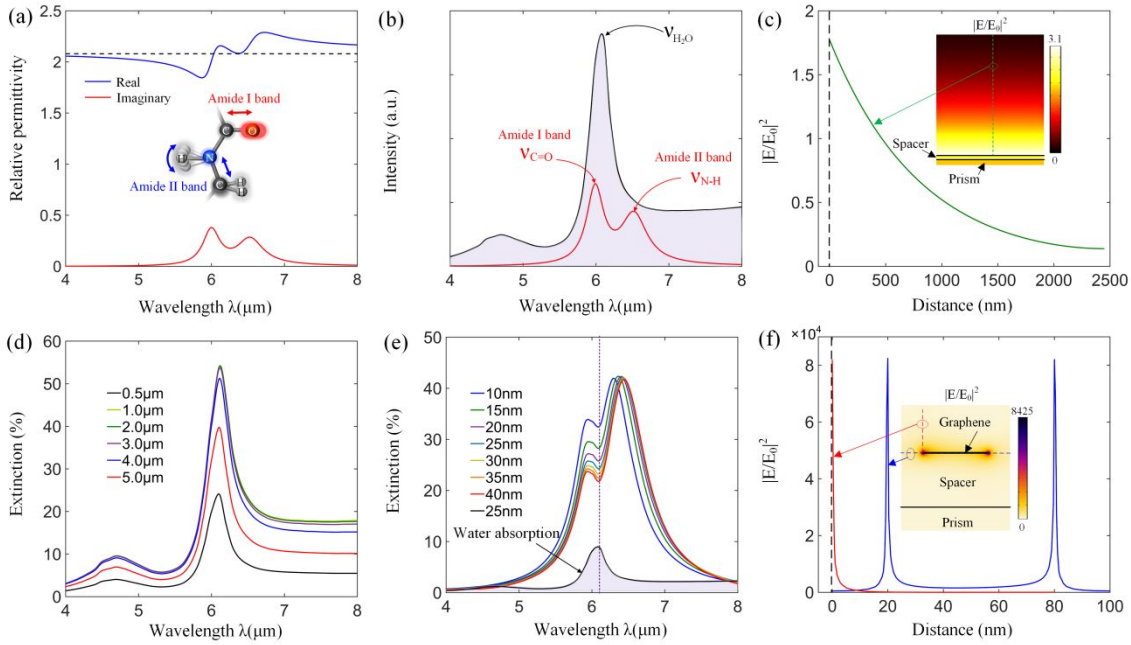

Figure 2 (a) Real and imaginary parts of the permittivity of a protein shown as blue and red line, respectively. The high-frequency, non-resonant term is shown as the dashed black line. The inset illustrates the molecular structure of the amide bond and associated vibrational modes (arrows). (b) Absorption spectra of protein (red line) and water (grey region) in infrared region. (c) Extracted E-field intensity along the green line from the electric field distribution of the prism in the inset. The incident angle is 40deg. (d) Simulated absorption spectra of water with different thickness on prism. (e) Simulated extinction infrared spectra of a graphene plasmonic antenna in water environment with different thickness. (f) Extracted E-field intensity from the electric field distribution of graphene nanoribbons in the inset along the direction parallel (blue line) and vertical (red line) to graphene nanoribbons.

incident angle of θ. The refractive index of spacer (n_s=1.45, Al_2O_3) is assumed to be smaller than that of the prism (n_p=2.4, ZnSe) such that attenuated total reflection can be occurred at the prism/spacer interface when θ is larger than the critical angle $\theta_{cs} \equiv \arcsin(n_s/n_p)$=37.2deg.

Extraction of the molecular fingerprints. The extinction spectra of the sensor with and without protein layer were calculated by R=100*(1-R_a/R_0), where R_0 is the background reflection spectra at Fermi energy of 0.001eV, R_a is the reflection spectra for a fixed graphene Fermi energy. Then the graphene plasmon-enhanced vibrational signals (Δ extinction) were extracted from the extinction spectra using the fitted spectra minus the original spectra. Finally, the peak Δ extinction is extracted as a function of wavelength, and further fitted using multi-peaks Lorentz line shape to obtain the absorption bands of molecules. The peaks were selected at the maximum Δ extinction, and the water absorption peak was selected at 6.10 μm for the cases when the molecules was dissolved in water environment (details can be seen in Supporting Information).

RESULTS AND DISCUSSION

Plasmonic behavior of the structure. The simulated resonant spectra are presented in Figure 1(b) when θ =40deg, Λ=100nm, W=50nm, t=50nm, E_f =0.4eV and μ_c =1000 $cm^2V^{-1}s^{-1}$. It can be seen that the transmission is totally blocked because ATR occurs at the prism/spacer interface as the incident angle $\theta>\theta_{cs}$. Additionally, an absorption peak (reflection dip) at 5.75 μm is observed in the absorption (reflection) spectrum due to the excitation of graphene plasmons in graphene nanoribbons. The resonant wavelength λ_{GPs} of graphene plasmons can be well predicted and calculated by

$$\lambda_{GPs} = \frac{\pi\hbar c}{e}\sqrt{\frac{2\times\xi\varepsilon_0(\varepsilon_a+\varepsilon_{eff})\Lambda}{NE_f}} \quad (2)$$

Here, ε_0 is the vacuum permittivity, ε_a is the relative permittivity of the air, ξ is a dimensionless fitting constant, and ε_{eff} is the effective permittivity of the spacer and prism when they are considered as an effective uniform medium, which can be approximately expressed as [45, 46]

$$\varepsilon_{eff} \equiv \varepsilon_s \frac{(\varepsilon_p+\varepsilon_s)\cdot\exp(2qt)+(\varepsilon_p-\varepsilon_s)}{(\varepsilon_p+\varepsilon_s)\cdot\exp(2qt)-(\varepsilon_p-\varepsilon_s)} \quad (3)$$

In Eq. (3), ε_p and ε_s are the relative dielectric constant of the prism and the spacer, q is the graphene plasmonic wavevector. According to Eq. 2 and 3, the resonant wavelength is calculated to be 5.75 μm with fitting constant of ξ = 2, which shows good agreement with the simulated result.

We then study the impact of the spacer (gating dielectric) thickness t on the plasmonic behavior of the sensing platform. The absorption mapping with varying spacer thickness t and incident wavelength λ is shown in Fig. 1(c) when the incident angle is fixed at θ=40 *deg*. The corresponding extracted the resonant wavelengths and absorptions are plotted as a function of the spacer thickness in Fig. S1. Obviously, the graphene plasmonic resonant wavelength blue shifts from 8.48 μm to 5.76 μm as t increases from 0 to 30 nm. This wavelength evolution can be attributed to the decrease of effective permittivity ε_{eff} beneath graphene with the increase of t, as indicated by Eq.2 and 3, thus resulting in the blue shift of the resonant wavelength. As t further increases to 100 nm, the resonant wavelength remains unchanged at 5.76 μm since the effective permittivity is nearly independence on t in this case (i.e., $(\varepsilon_p+\varepsilon_s)\exp(2qt) >> \varepsilon_p-\varepsilon_s$ in Eq. (3). Such evolution of resonant wavelength with varying t can be well reproduced by Eq. 2 and 3, as shown as the star yellow line in Fig. 1(c). Another important observation from Fig. S1 is that the resonant absorption is also nearly independent of the spacer thickness. The insensitivity of graphene plasmonic response of the sensor on spacer thickness points to a facile way to its practical realization.

Graphene plasmonic ATR-SEIRAS. The principle of the proposed graphene plasmonic based ATR-SEIRAS for detection of molecules in aqueous solution is illustrated in Figure 2. The recombinant protein A/G and goat anti-mouse immunoglobulin G (IgG) are used as the sensing analyte. The real and imaginary parts of complex permittivity are shown in Figure 2(a), which is evaluated by Drude-Lorentz type dispersion[32] as

$$\varepsilon(\omega) = \varepsilon_\infty + \sum_{k=1}^{2} \frac{S_k^2}{\omega_k^2 - \omega^2 - i\omega\gamma_k} \quad (4)$$

In Eq. 4, ε_∞=2.08 is the high-frequency, non-resonant term (dashed line in Figure 2(a)), ω_1=1669cm^{-1} and ω_2=1532cm^{-1} are the vibrational frequencies of the Amide I and II bands, γ_1=78.1cm^{-1}, γ_2=101cm^{-1}, S_1=213cm^{-1}, S_2=200cm^{-1}. Based on this parameter, the simulated intrinsic absorption spectrum of the protein layer is shown as the red line in Figure 2(b). Two absorption peaks located at 1669 cm^{-1} (5.99 μm) and 1532 cm^{-1} (6.53 μm) can be observed, corresponding to the vibrational fingerprints of amide I band and II band, respectively. These two absorption bands are primarily associated with the C=O stretch mode and N-H bend mode in the amide functional group as illustrated in the inset of Figure 2(a). By detecting these vibrational modes from the infrared fingerprint spectrum, we can quantitatively and qualitatively recognize the chemical groups inside molecules so as to identify the species of the molecules. Whereas when the molecules are dissolved in the aqueous solution (common situation for bioanalysis), these vibrational modes would be difficult to distinguish from the fingerprint spectrum for the traditional infrared spectroscopy, because the water itself has very strong absorption in the infrared frequencies. As an illustration, we simulated the absorption spectrum of liquid water accounting for its frequency-dispersive complex refractive index [47], shown as the grey region in Figure 2(b). We can observe a large absorption band associated with the OH-bending mode of water located at 1640 cm^{-1} (6.10 μm), which is overlapped with the vibrational fingerprints of protein. This makes it difficult to avoid the large background water absorption when detecting the protein in aqueous solution.

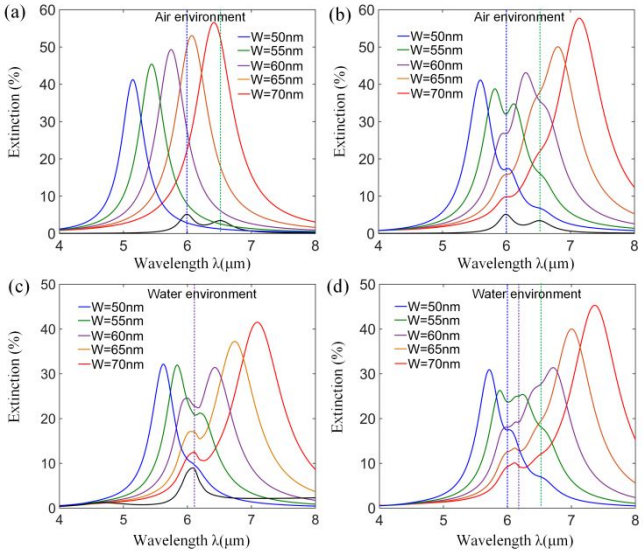

Figure 3 Extinction spectra of graphene nanoribbons arrays with different widths (a) before and (b) after coating with protein in dry (air) environment. An enlarged (10-fold) intrinsic absorption spectrum of 8nm protein is also displayed at the bottom of the figure a and b. Extinction spectra of graphene nanoribbons arrays with different widths (c) before and (d) after coating with protein in water environment. The spectrum of water is also displayed at the bottom of the figure c.

Our strategy to suppress the background water absorption is employing highly confined graphene plasmons combined with an ATR configuration. For the ATR configuration without graphene nanoribbons, the electric field intensity extracted from the electric field distribution is plotted in Figure 2(c). It can be seen that electric field decays exponentially into the sensing sample, with a characteristic penetration depth (for 1/e drop in intensity) of ~1.25 μm. Such shallow penetration depth enables the highly sensitive detection of target molecules dissolved even in the strongly infrared absorbing solution (such as water). As shown in Figure 2(d), the background absorption of water is nearly unchanged when the thickness of water is larger than 3μm. Therefore, the signal from the bulk water molecules can be effectively suppressed in ATR configuration compared to that in traditional transmission configuration or Fabry-Perot reflection configuration (Figure S2).

For the proposed graphene plasmonic based ATR-SEIRAS configuration, the graphene plasmon with localized near-field enhancement can further confine the surface electric field into subwavelength space, shrinking the penetration depth into the nanometer level and suppressing the infrared absorption of water. As shown in Fig. 2(f), the electric field is highly confined at the tip ends of graphene plasmonic nanoribbons with near-field enhancement of 8.4×10^3, which is much larger than that of the metallic nanoantenna[38]. The intensity of electric field at the

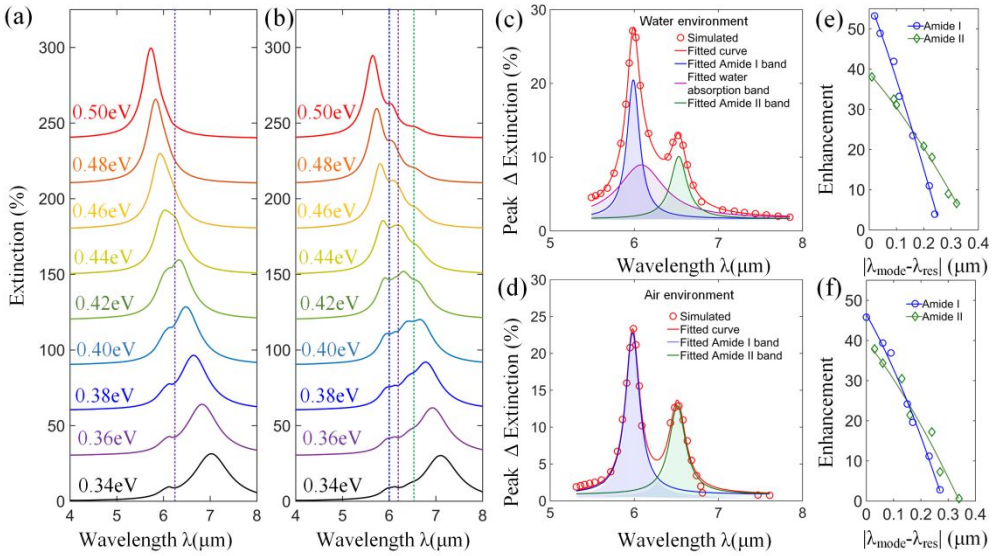

Figure 4 (a) Extinction spectra of the graphene nanoribbon array at varied Fermi energy in water environment. (b) Extinction spectra of the graphene nanoribbon array coated with an 8-nm protein film at varied Fermi energy in water environment. The dashed lines in (a) and (b) indicate the positions of vibrational modes of water and the protein molecules. The Lorentz fitted protein absorption enhanced by graphene plasmons in (c) water and (d) air environment. Calculated enhancement of the vibrational fingerprints of proteins at amide I and II bands in (e) water and (f) air environment.

graphene nanoribbon tip end decays exponentially along the direction vertical to graphene (red line). While along the direction parallel to graphene (blue line), the electric field intensity is moderate in graphene nanoribbons but decays rapidly after passing the tip end, indicating an excellent surface selectivity. The extinction spectra of graphene plasmon in water with varying thickness is shown in Figure 2(e) (calculation details of the extinction spectra can be seen in Figure S3). We can observe a dip on the graphene plasmonic resonant peak, which is induced by the strong coupling between the OH-bending mode of water molecules and the graphene plasmonic mode. The dip becomes more obvious as the coupling becomes stronger with the increased thickness of water from 10 nm to 40nm. Whereas the dip is almost unchanged as the thickness is further increased. This indicates that the effect of the water absorption on the graphene plasmon can be neglected when the thickness of water is larger than 40nm, owing to the highly confined electromagnetic field at the graphene surface. This provides the opportunity to detect biomolecules absorbed at the graphene surface in aqueous solution, without concerning for the length of optical path.

Detection of protein molecules in aqueous solution. To illustrate the application of graphene plasmonic based ATR-SEIRAS for bioanalysis, we first simulate the detection of a protein layer (thickness of 8nm) in air and aqueous environments. Comparing simulations in the two kinds of environments allows us to investigate the influence of the water absorption on the plasmonic response and performance of the sensing platform.

The extinction spectra of the graphene nanoribbons without protein coating in air are shown in Figure 3(a). An enlarged (10-fold) intrinsic absorption spectrum of the 8 nm protein layer is also provided as the black line. It is observed that prominent plasmonic resonant peak red shifts with increased width, which covers the absorption band of the protein. The extinction spectra of the graphene nanoribbons after coating a protein layer is shown in Figure 3(b). Obviously, the intrinsic absorption of the ultrathin protein layer is very low (only 0.54%), which is attributed to the weak light-molecule interaction induced by the huge scale mismatch between microscale infrared light and the nanoscale molecules. When the molecules are adsorbed on the graphene nanoribbons surface, the weak vibrational modes are significantly enhanced by coupling with graphene plasmons, which exhibit obvious dips associated with the amide bands over the resonant peaks. These observed dips are the consequence of the destructive interference when the graphene plasmonic mode and molecular vibrational modes interact with an opposite phase relationship. This highlights the possible practical application of the ATR-SEIRAS sensing platform for the detection of ultra-thin molecular film.

Similar simulations are readily performed in aqueous solution, as illustrated in Figure 3(c-d). The water vibrational band exhibits clear impact on the extinction spectra of the configuration, as present in Figure 3(c) (the black line represents the absorption spectrum of water for comparison). Obvious dips induced by the present of water molecules (OH-bending mode) can be observed over the resonant peak with respect to the extinction spectra in air environment. When the protein layer is further absorbed at the graphene surface, extinction spectra with obvious dips induced by molecular vibrational modes still can be achieved in the aqueous environment, as shown in Fig. 3(d). The slight decrease of the vibrational signal and broadening of the extinction spectra can be attributed to the increased plasmonic damping by the present of the water absorption band. Yet, the vibrational signal is still significantly improved compared to the intrinsic absorption of protein layer without plasmonic enhancement, indicating that the proposed graphene plasmonic based ATR-SEIRAS can be

employed to detect the protein molecules in aqueous solution.

Tunable and selective detection of protein molecules in aqueous solution. The electrical tunable graphene plasmon by external gate voltage enables the detection of thin molecular films with several molecular vibrational modes on the same sensor, which is unavailable for the traditional metallic plasmons. Combining this feature and the proposed ATR configuration, we can resolve the chemical fingerprints of molecules in the aqueous solution by sweeping the graphene Fermi energy.

The extinction spectra of sensor with varying Fermi energy E_f in water and air environment are shown in Figure 4(a) and Figure S4, respectively. Compared to the case in air environment, a dip associated with the H_2O-bending mode can be observed on the graphene plasmonic peaks in the water environment, which blue shifts from 7.05 μm to 5.73 μm as E_f increases from 0.34 eV to 0.50 eV. After coating with 8nm protein layer, the curves exhibit a slight red-shifting, which results from the plasmonic resonance in response to the non-resonant, high-frequency (n~1.45) component of the refractive index of the protein layer. Moreover, obvious dips associated with the amide bands can be observed in these spectra with neglected effect of water absorption band. These dips vary in strength and line shape, depending on their vibrational wavelength relative to the graphene plasmonic resonant wavelength. By tuning the graphene Fermi energy, the dips become progressively more intense with increasing spectral overlap between the graphene plasmonic resonance and the molecular vibrational bands. Similar phenomenon also can be observed for the case in air environment (Figure S5 (a)). Therefore, the proposed configuration offers unique frequency-selective enhancement for individual molecular vibrational mode.

In order to visually reveal the frequency-selective enhancement effect and resolve the fingerprints of protein molecules, the enhanced vibrational signals (Δ extinction) of protein molecules are further extracted from the extinction spectra (details can be seen in Figure S5 and Figure S6). Obviously, the amplitude of vibrational signal close to the resonant peak of graphene plasmons is much larger than that of those wing signals, as shown in Figure S7. The maximum signal strength of amide I and II modes are 27.1% and 12.9% in water environment when the graphene Fermi energy are 0.47 eV and 0.41 eV, respectively, which are about 53 and 38 times with respect to their intrinsic absorption (0.51% and 0.34%) without resonance enhancement. The peak Δ extinction with varying Fermi energy is further extracted from Figure S7 and plotted in Figure 4(c) and 4(d) for water and air environment, respectively. The multi-peaks Lorentz fitted absorption spectra of protein molecules enhanced by graphene plasmons show excellent agreement with the simulation results as well as the intrinsic absorption spectrum for both cases. Based on these fitted curves, the absorption bands of Amide I, Amide II and water can be achieved (shown as the blue, green and purple regions in the figures) with central wavelength located at exactly the resonant wavelengths of these vibrational modes. We further show that the multiple vibrational modes also can be resolved as the resonance is broadened to the longer wavelength region (8~12 μm) using the same device, benefit from the wideband tunable plasmonic response of the configuration, as shown in Figure S8-S10. Therefore, the fingerprints of molecules can be resolved by sweeping the graphene Fermi energy in a wide wavelength ranged from 5~12μm, even for the vibrational modes that is very closed to the water absorption mode, indicating promising applications for the proposed sensing platform in bioanalysis.

The calculated enhancement factors of the molecular vibrational modes in water and air environment are plotted in Fig. 4(e) and 4(f), respectively, as a function of the wavelength difference ($|\lambda_{mode}-\lambda_{res}|$) between the molecular vibrational absorption wavelength and graphene plasmonic resonant wavelength. It can be seen that the enhancement factor is inversely proportional to the wavelength detuning, which follows the basic principle of plasmon-enhanced infrared spectroscopy. This result suggests that the vibrational modes can be selectively enhanced employing the wideband tunable graphene plasmons. For instance, the enhancement factor of the amide I mode in water environment can be improved from 4 to 53 via tuning resonant wavelength by adjusting graphene Fermi energy.

Improved enhancement by improving the mode energy. The above analysis indicates that the combination of graphene plasmons and ATR configuration can resolve the vibrational modes of aqueous molecules with ultrahigh sensitivity in a wide waveband. Despite of this, there is still plenty of room for the improvement of the enhancement factor. It has been demonstrated that the enhancement of SEIRAS is proportional to the square of the amplitude of local electric field, which can be expressed as [48]

$$|E|^2 = C\frac{W}{V} = C\frac{P_{in}A\tau}{V} \quad (5)$$

where E is the amplitude of electric field, C is a constant that depends on a specific mode, V is the mode volume of the graphene plasmonic mode, W is the mode energy of a graphene plasmonic mode determined by the incident power P_{in}, the absorption rate A, and the electron relaxation time of graphene τ. According to Eq. (5), a higher absorption and a larger relaxation time can result in the higher mode energy, which could induce a larger local electric field to enhance the SEIRA signal. For the proposed configuration, the absorption can be adjusted by tuning the incident angle, while the relaxation time can be modulated by tuning the graphene mobility. Therefore, we further improve the mode energy of graphene plasmons to obtain the maximum enhancement factor by optimizing the incident angle and graphene mobility in this section.

For the proposed configuration, the resonant wavelength of the graphene plasmons is nearly unchanged with varying incident angles, while the absorption of graphene plasmons has a strong dependence on the incident angle, which offers a useful degree of freedom to manipulate the plasmonic response of the sensing platform (details can be seen in Figure S11). To perform the SEIRAS measurement in water environment, the configuration is considered to be operate under ATR condition, and the Fermi energy are chosen to be 0.47eV and 0.41eV for Amide I and II band, respectively. Under this consideration, the molecular vibrational modes

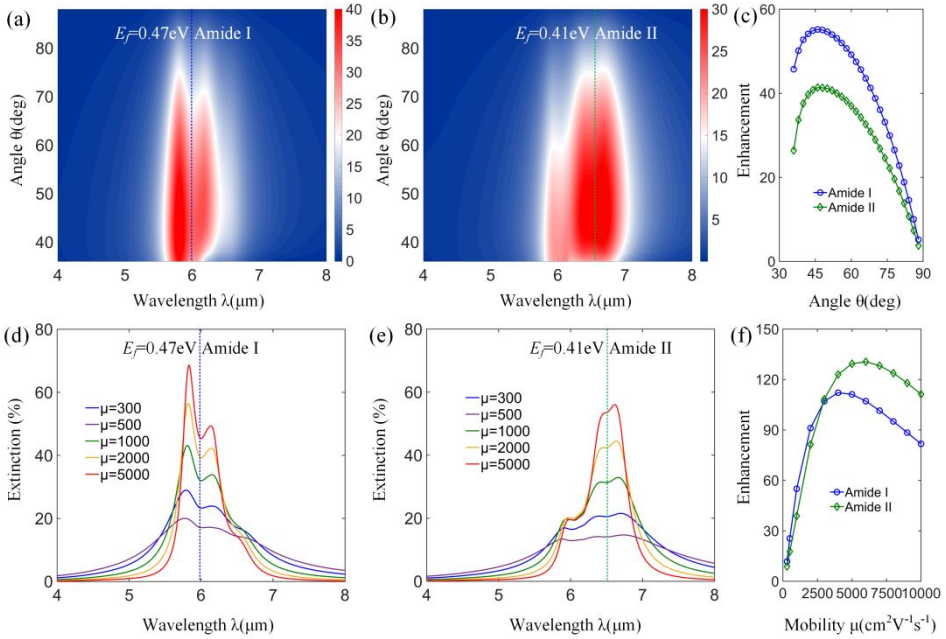

Figure 5 Extinction spectra of graphene nanoribbons coated with 8nm protein mapping with varying incident angle when the graphene Fermi energy is (a) 0.47eV and (b) 0.41eV in water environment. (c) Calculated enhancement of the amide I and II vibrational modes as function of the incident angle. Extinction spectra of graphene nanoribbons coated with 8nm protein mapping with varying graphene mobility when the graphene Fermi energy is (d) 0.47eV and (e) 0.41eVin water environment. (f) Calculated enhancement of the amide I and II vibrational modes as function of the graphene mobility.

and graphene plasmonic modes can be spectrally matched, so we can achieve the maximum enhancement of Amide I and II band according the results discussed above. It is intuitively observed from Figure 5(a) and 5(b) that the strong interaction between the molecule vibrational modes and the graphene plasmonic mode leads to the splitting of the infrared extinction spectra at the position of the molecules absorption lines, which significantly enhances the vibrational signal of Amide I and II bands. Moreover, the water absorption band is nearly invisible from the extinction mapping, indicating the highly reliable detection of molecules in water environment. The corresponding calculated enhancement factor as a function of incident angles for Amide I and II bands are plotted in Figure 5(c). It shows that the enhancement factor first increases and then decreases after reaching the maximum value as the incident angle increases from 35*deg* to 89*deg*. The maximum enhancement factors are estimated to be 55 and 42 for Amide I and II bands, respectively, both at the incident angle of 46*deg* since the maximum absorption is achieved at this condition, which is in accordance with Eq. 5. This point to a feasible way to achieve the optimized enhancement factor of the molecular vibrational signal in practice.

We finally investigate the effect of graphene mobility on the enhancement factor. It has been demonstrated that graphene mobility of 200,000 $cm^2V^{-1}s^{-1}$ could be obtained in high-quality suspended graphene[49], while that could reach 40,000 $cm^2V^{-1}s^{-1}$ on the SiO_2 substrate at room temperature[50]. Here, we consider the easily available CVD-growth graphene with mobility in a range from 300 to 10,000 $cm^2V^{-1}s^{-1}$. The extinction spectra with varying graphene mobility for Fermi energy of 0.47eV and 0.41eV are shown in Figure 5(d) and 5(e), respectively. It can be seen that high-quality extinction spectra of protein molecules in water environment can be still achieved even when the graphene mobility is reduced down to only 300 $cm^2V^{-1}s^{-1}$. Additionally, the extinction dips become more obvious as the mobility increases, indicating the stronger interaction between molecular vibrational modes and graphene plasmonic modes. The corresponding calculated enhancement factor as a function of graphene motilities are plotted in Figure 5(f). Maximum enhancement factors of 112 and 130 can be obtained for Amide I and II bands at around 5,000 $cm^2V^{-1}s^{-1}$. The slight decrease of the enhancement for the large mobility can be understood that the absorption is reduced though the mobility further increases (Figure S12). Noted from Eq. 5 that the enhancement factor is still far from reaching the limit and can be further improved. On one hand, the quality factor of the extinction spectra could be increased by optimizing the structural parameter of the sensor to make sure that the sensor achieves a higher absorption at a higher graphene mobility. On the other hand, we can employ higher order graphene plasmonic modes to reduce the mode volume *V*, which would also lead to larger local electric fields and hence higher enhancement factors.

CONCLUSIONS

In conclusion, we propose a wideband tunable graphene plasmon-enhanced infrared biosensor to detect the aqueous-phase molecules. By combining the near-field enhancement effect of graphene plasmon with attenuated total reflection effect in an Otto prism configuration, the water background absorption can be effectively suppressed, enabling us to detect and extract the chemical fingerprints of biomolecules in aqueous environment. It is found that the fingerprints of protein molecules can be selectively enhanced and resolved by sweeping the

graphene Fermi energy without the interference from the aqueous environment. By further optimizing the incident angle and graphene mobility to improve the mode energy of graphene plasmons, the maximum enhancement factor can reach 112 and 130 for Amide I and II bands of the protein molecules in water environment. Such sensing platform with impressive performance expands the applications of graphene plasmons for the identification of biomolecules interactions in aqueous solution.

ASSOCIATED CONTENT

Supporting Information. The Supporting Information is available free of charge via the Internet at http://pubs.acs.org.

(S1) Effect of the spacer thickness on the resonant wavelength and absorption. (S2) Comparison of the background water absorption in different configurations. (S3) Calculation of the extinction spectra in water environment. (S4) Extracted vibrational signals from the extinction spectra. (S5) Resolving the molecular fingerprint in a wider wavelength region. (S6) Effect of the incident angle and graphene mobility on the plasmonic response.

AUTHOR INFORMATION

Corresponding Authors

* E-mail: tll@cigit.ac.cn (L.L.T.)
* E-mail: wwei@cqu.edu.cn (W.W.)

Author Contributions

The manuscript was written through contributions of all authors. All authors have given approval to the final version of the manuscript.

Notes

The authors declare no competing financial interest.

ACKNOWLEDGMENT

This research was funded by National Natural Science Foundation of China (No. 61875025, 61675037), Chongqing Research Program of Basic Research and Frontier Technology (cstc2017jcyjBX0048, cstc2017jcyjBX0054), and Fundamental Research Funds for the Central Universities (2018CDQYGD0022, cqu2018CDHB1B03).

REFERENCES

(1) Yang, X.; Sun, Z.; Low, T.; Hu, H.; Guo, X.; Garcia de Abajo, F. J.; Avouris, P.; Dai, Q., Nanomaterial-Based Plasmon-Enhanced Infrared Spectroscopy. *Adv. Mater.* **2018**, e1704896.

(2) Neubrech, F.; Huck, C.; Weber, K.; Pucci, A.; Giessen, H., Surface-Enhanced Infrared Spectroscopy Using Resonant Nanoantennas. *Chem. Rev.* **2017,** *117*, 5110-5145.

(3) Liu, L.; Ji, M.; Dong, Y.; Zhang, R.; Buchroithner, M., Quantitative Retrieval of Organic Soil Properties from Visible Near-Infrared Shortwave Infrared (Vis-NIR-SWIR) Spectroscopy Using Fractal-Based Feature Extraction. *Remote Sens.* **2016,** *8* (12), 1035.

(4) Wain, A. J.; O'Connell, M. A., Advances in surface-enhanced vibrational spectroscopy at electrochemical interfaces. *Advances in Physics: X* **2017,** *2* (1), 188-209.

(5) Baranov, D. G.; Wersäll, M.; Cuadra, J.; Antosiewicz, T. J.; Shegai, T., Novel Nanostructures and Materials for Strong Light–Matter Interactions. *ACS Photonics* **2017,** *5* (1), 24-42.

(6) Mayerhöfer, T. G.; Popp, J., Periodic array-based substrates for surface-enhanced infrared spectroscopy. *Nanophotonics* **2018,** *7* (1), 39-77.

(7) Weber, K.; Nesterov, M. L.; Weiss, T.; Scherer, M.; Hentschel, M.; Vogt, J.; Huck, C.; Li, W.; Dressel, M.; Giessen, H.; Neubrech, F., Wavelength Scaling in Antenna-Enhanced Infrared Spectroscopy: Toward the Far-IR and THz Region. *ACS Photonics* **2016,** *4* (1), 45-51.

(8) Wang, T.; Dong, Z.; Koay, E. H. H.; Yang, J. K. W., Surface-Enhanced Infrared Absorption Spectroscopy Using Charge Transfer Plasmons. *ACS Photonics* **2019,** *6* (5), 1272-1278.

(9) Cerjan, B.; Yang, X.; Nordlander, P.; Halas, N. J., Asymmetric Aluminum Antennas for Self-Calibrating Surface-Enhanced Infrared Absorption Spectroscopy. *ACS Photonics* **2016,** *3* (3), 354-360.

(10) Wallace, G. Q.; Tabatabaei, M.; Hou, R.; Coady, M. J.; Norton, P. R.; Simpson, T. S.; Rosendahl, S. M.; Merlen, A.; Lagugné-Labarthet, F., Superimposed Arrays of Nanoprisms for Multispectral Molecular Plasmonics. *ACS Photonics* **2016,** *3* (9), 1723-1732.

(11) Wei, W.; Chen, N.; Nong, J.; Lan, G.; Wang, W.; Yi, J.; Tang, L., Graphene-assisted multilayer structure employing hybrid surface plasmon and magnetic plasmon for surface-enhanced vibrational spectroscopy. *Opt. Express* **2018,** *26* (13), 16903.

(12) Chen, K.; Dao, T. D.; Ishii, S.; Aono, M.; Nagao, T., Infrared Aluminum Metamaterial Perfect Absorbers for Plasmon-Enhanced Infrared Spectroscopy. *Adv. Funct. Mater.* **2015,** *25* (42), 6637-6643.

(13) Novoselov, K. S.; Fal'ko, V. I.; Colombo, L.; Gellert, P. R.; Schwab, M. G.; Kim, K., A roadmap for graphene. *Nature* **2012,** *490* (7419), 192-200.

(14) Grigorenko, A. N.; Polini, M.; Novoselov, K. S., Graphene plasmonics. *Nat. Photonics* **2012,** *6* (11), 749-758.

(15) Huang, S.; Song, C.; Zhang, G.; Yan, H., Graphene plasmonics: physics and potential applications. *Nanophotonics* **2017,** *6* (6), 1191-1204.

(16) Brar, V. W.; Jang, M. S.; Sherrott, M.; Lopez, J. J.; Atwater, H. A., Highly confined tunable mid-infrared plasmonics in graphene nanoresonators. *Nano Lett.* **2013,** *13* (6), 2541-7.

(17) García de Abajo, F. J., Graphene Plasmonics: Challenges and Opportunities. *ACS Photonics* **2014,** *1* (3), 135-152.

(18) Guo, Q.; Li, C.; Deng, B.; Yuan, S.; Guinea, F.; Xia, F., Infrared Nanophotonics Based on Graphene Plasmonics. *ACS Photonics* **2017,** *4* (2), 2989–2999.

(19) Politano, A.; Chiarello, G., Plasmon modes in graphene: status and prospect. *Nanoscale* **2014,** *6* (19), 10927-40.

(20) Nong, J.; Tang, L.; Lan, G.; Luo, P.; Guo, C.; Yi, J.; Wei, W., Wideband tunable perfect absorption of graphene plasmons via attenuated total reflection in Otto prism configuration. *Nanophotonics* **2020,** *9* (3), 645-655.

(21) Fang, Z.; Wang, Y.; Schlather, A. E.; Liu, Z.; Ajayan, P. M.; Garcia de Abajo, F. J.; Nordlander, P.; Zhu, X.; Halas, N. J., Active tunable 002.absorption enhancement with graphene nanodisk arrays. *Nano Lett.* **2014,** *14* (1), 299-304.

(22) Kim, S.; Jang, M. S.; Brar, V. W.; Mauser, K. W.; Kim, L.; Atwater, H. A., Electronically Tunable Perfect Absorption in Graphene. *Nano Lett.* **2018,** *18* (2), 971-979.

(23) Hu, H.; Zhai, F.; Hu, D.; Li, Z.; Bai, B.; Yang, X.; Dai, Q., Broadly tunable graphene plasmons using an ion-gel top gate with low control voltage. *Nanoscale* **2015,** *7* (46), 19493-500.

(24) Nong, J.; Wei, W.; Wang, W.; Lan, G.; Shang, Z.; Yi, J.; Tang, L., Strong coherent coupling between graphene surface plasmons and anisotropic black phosphorus localized surface plasmons. *Opt. Express* **2018,** *26* (2), 1633-1644.

(25) Wei, W.; Nong, J.; Tang, L.; Zhang, G.; Yang, J.; Luo, W., Conformal Graphene-Decorated Nanofluidic Sensors Based on Surface Plasmons at Infrared Frequencies. *Sensors* **2016,** *16* (6).

(26) Yao, B.; Liu, Y.; Huang, S.-W.; Choi, C.; Xie, Z.; Flor Flores, J.; Wu, Y.; Yu, M.; Kwong, D.-L.; Huang, Y.; Rao, Y.; Duan, X.; Wong, C. W., Broadband gate-tunable terahertz plasmons in graphene heterostructures. *Nat. Photonics* **2017**.
(27) Safaei, A.; Chandra, S.; Leuenberger, M. N.; Chanda, D., Wide Angle Dynamically Tunable Enhanced Infrared Absorption on Large-Area Nanopatterned Graphene. *ACS Nano* **2019,** *13* (1), 421-428.
(28) Li, Y.; Yan, H.; Farmer, D. B.; Meng, X.; Zhu, W.; Osgood, R. M.; Heinz, T. F.; Avouris, P., Graphene plasmon enhanced vibrational sensing of surface-adsorbed layers. *Nano Lett.* **2014,** *14* (3), 1573-7.
(29) Peng, L.; Zhang, L.; Yuan, J.; Chen, C.; Bao, Q.; Qiu, C. W.; Peng, Z.; Zhang, K., Gold nanoparticle mediated graphene plasmon for broadband enhanced infrared spectroscopy. *Nanotechnology* **2017,** *28* (26), 264001.
(30) Sun, J.; Chen, Z.; Yuan, L.; Chen, Y.; Ning, J.; Liu, S.; Ma, D.; Song, X.; Priydarshi, M. K.; Bachmatiuk, A.; Rummeli, M. H.; Ma, T.; Zhi, L.; Huang, L.; Zhang, Y.; Liu, Z., Direct Chemical-Vapor-Deposition-Fabricated, Large-Scale Graphene Glass with High Carrier Mobility and Uniformity for Touch Panel Applications. *ACS Nano* **2016,** *10* (12), 11136-11144.
(31) Lee, I. H.; Yoo, D.; Avouris, P.; Low, T.; Oh, S. H., Graphene acoustic plasmon resonator for ultrasensitive infrared spectroscopy. *Nat. Nanotechnol.* **2019,** *14* (4), 313-319.
(32) Rodrigo, D.; Limaj, O.; Janner, D.; Etezadi, D.; Abajo, F. J. G. d.; Pruneri, V.; Altug, H., Mid-infrared plasmonic biosensing with graphene. *Science* **2015,** *349* (6244), 165-168.
(33) Zhang, K.; Zhang, L.; Yap, F. L.; Song, P.; Qiu, C. W.; Loh, K. P., Large-Area Graphene Nanodot Array for Plasmon-Enhanced Infrared Spectroscopy. *Small* **2016,** *12* (10), 1302-8.
(34) Hu, H.; Yang, X.; Guo, X.; Khaliji, K.; Biswas, S. R.; Garcia de Abajo, F. J.; Low, T.; Sun, Z.; Dai, Q., Gas identification with graphene plasmons. *Nat. Commun.* **2019,** *10* (1), 1131.
(35) Farmer, D. B.; Avouris, P.; Li, Y.; Heinz, T. F.; Han, S.-J., Ultrasensitive Plasmonic Detection of Molecules with Graphene. *ACS Photonics* **2016,** *3* (4), 553-557.
(36) Zheng, B.; Yang, X.; Li, J.; Shi, C. F.; Wang, Z. L.; Xia, X. H., Graphene Plasmon-Enhanced IR Biosensing for in Situ Detection of Aqueous-Phase Molecules with an Attenuated Total Reflection Mode. *Anal. Chem.* **2018,** *90* (18), 10786-10794.
(37) Rodrigo, D.; Tittl, A.; Limaj, O.; Abajo, F. J. G. d.; Pruneri, V.; Altug, H., Double-layer graphene for enhanced tunable infrared plasmonics. *Light Sci. Appl.* **2017,** *6* (6), e16277.
(38) Adato, R.; Altug, H., In-situ ultra-sensitive infrared absorption spectroscopy of biomolecule interactions in real time with plasmonic nanoantennas. *Nat. commun.* **2013,** *4*, 2154.
(39) Rodrigo, D.; Tittl, A.; Ait-Bouziad, N.; John-Herpin, A.; Limaj, O.; Kelly, C.; Yoo, D.; Wittenberg, N. J.; Oh, S. H.; Lashuel, H. A.; Altug, H., Resolving molecule-specific information in dynamic lipid membrane processes with multi-resonant infrared metasurfaces. *Nat. commun.* **2018,** *9* (1), 2160.
(40) Cao, F.; Wu, L.; Ruan, Y.; Bai, J.; Jiang, X., In Situ Surface-Enhanced Infrared Absorption Spectroscopy of Aqueous Molecules with Facile-Prepared Large-Area Reduced Graphene Oxide Island Film. *Anal. Chem.* **2018,** *90* (11), 6526-6531.
(41) Hu, Y.; López-Lorente, Á. I.; Mizaikoff, B., Versatile Analytical Platform Based on Graphene-Enhanced Infrared Attenuated Total Reflection Spectroscopy. *ACS Photonics* **2018,** *5* (6), 2160-2167.
(42) Wei, W.; Nong, J.; Zhu, Y.; Tang, L.; Zhang, G.; Yang, J.; Huang, Y.; Wei, D., Cavity-enhanced continuous graphene plasmonic resonator for infrared sensing. *Opt. Commun.* **2017,** *395*, 147-153.
(43) Chu, H.-S.; How Gan, C., Active plasmonic switching at mid-infrared wavelengths with graphene ribbon arrays. *Appl. Phys. Lett.* **2013,** *102* (23), 231107.
(44) Koppens, F. H.; Chang, D. E.; Garcia de Abajo, F. J., Graphene plasmonics: a platform for strong light-matter interactions. *Nano Lett.* **2011,** *11* (8), 3370-3377.
(45) Wei, W.; Nong, J.; Tang, L.; Zhu, Y.; Shi, H., Coupling of Graphene Plasmonics Modes Induced by Near-Field Perturbation at Terahertz Frequencies. *Plasmonics* **2016,** *11* (4), 1109-1118.
(46) Tang, L.; Du, J.; Du, C.; Zhu, P.; Shi, H., Scaling phenomenon of graphene surface plasmon modes in grating-spacer-graphene hybrid systems. *Opt. Express* **2014,** *22* (17), 20214-22.
(47) Hale, G. M.; Querry, M. R., Optical Constants of Water in the 200-nm to 200-μm Wavelength Region. *Appl. Opt.* **1973,** *12*, 555-563.
(48) Tang, L.; Nong, J.; Wei, W.; Zhang, S.; Zhu, Y.; Shang, Z.; Yi, J.; Wang, W., Mode energy of graphene plasmons and its role in determining the local field magnitudes. *Opt. Express* **2018,** *26* (5), 6214.
(49) Bolotin, K. I.; Sikes, K. J.; Jiang, Z.; Klima, M.; Fudenberg, G.; Hone, J.; Kim, P.; Stormer, H. L., Ultrahigh electron mobility in suspended graphene. *Solid State Commun.* **2008,** *146* (9-10), 351-355.
(50) Chen, J. H.; Jang, C.; Xiao, S.; Ishigami, M.; Fuhrer, M. S., Intrinsic and extrinsic performance limits of graphene devices on SiO2. *Nat. nanotechnol.* **2008,** *3* (4), 206-9.

For Table of Contents Only